ACS APPLIED MATERIALS & INTERFACES

www.acsami.org

Research Article

Nanopore Generation in Biodegradable Silk/Magnetic Nanoparticle Membranes by an External Magnetic Field for Implantable Drug Delivery

Ya Wang, Giovanni Boero, Xiaosheng Zhang, and Juergen Brugger*

Cite This: *ACS Appl. Mater. Interfaces* 2022, 14, 40418–40426

Read Online

ACCESS | Metrics & More | Article Recommendations | Supporting Information

ABSTRACT: Implantable devices for localized and controlled drug release are important, e.g., for therapies of cancer and chronic pain. However, most of the existing active implants are limited by the usage of nonbiodegradable materials; thus, surgery is needed to extract them after the treatment, which leads to secondary damage. Here, we show a fully biodegradable composite membrane made from silk fibroin and magnetic nanoparticles (MNPs). The membrane porosity can be remotely modified by an alternating magnetic field, which opens nanopores by local heating of MNPs in the composite allowing a liquid to diffuse through them. The stability of the silk membrane in water can be prolonged up to several months by increasing its β-sheet content through ethanol annealing. We present the following original findings. (a) Nanopores can be generated inside the silk/MNP composite membrane by exposing it to an external alternating magnetic field. (b) A longer exposure time results in more nanopore sites. (c) The controllable release of rhodamine B dye is achieved by tuning the period of exposure to the magnetic field. The obtained results demonstrate the suitability of the investigated silk/MNP composite membrane as a potential functional material for implantable drug delivery.

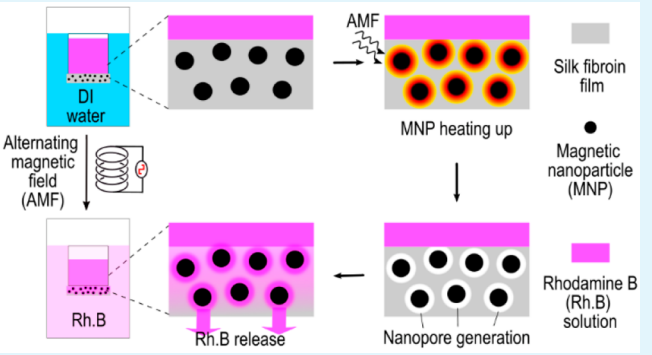

KEYWORDS: *nanopore, silk fibroin, magnetic nanoparticles, biodegradability, implantable drug delivery*

INTRODUCTION

Implantable drug delivery systems can provide localized drug release in precisely controlled, patient-specific time sequences with a single administration.[1] By now, various kinds of drug delivery implants have been successfully developed for the treatment of chronic pain,[2,3] osteoporosis,[4] retinal diseases,[5] ovarian cancer,[6] prostate cancer,[7] and brain tumor.[8] However, most of the existing implants need to be removed surgically after the treatment period or replaced after the device's lifetime, which leads to additional costs, secondary injuries, and higher risks of postsurgical complications such as inflammation, infection, and pain. To prevent such complications, biodegradable drug delivery implants, which degrade in the human body without harmful residues, would be a considerable improvement for controllable in vivo drug administration systems.[9,10]

Silk fibroin is a natural protein with beneficial properties for implantable drug delivery such as controllable biodegradation,[11] biocompatibility,[12] all-aqueous purifications,[13] versatile processing,[14] compatibility with sterilization methods,[15] and excellent mechanical properties.[16] Additionally, membranes prepared from silk fibroin can be used for biomedical applications, including tissue engineering,[17,18] wound healing,[19] implants for delivering therapeutics such as enzymes and drugs,[20,21] and as a solid matrix to encapsulate blood analytes[22] and antioxidants.[23] In addition to bare silk fibroin, silk fibroin membranes with incorporated nanoparticles have also been investigated for biomedical applications. Hu et al. developed gold nanoparticle-doped silk membranes, which could be activated by light to power implanted microdevices.[24] Because the depth of penetration of light into a tissue is limited to 1−6 mm depending on the wavelength used, this approach is not suitable for deep tissue applications in vivo. Furthermore, compounds such as melanin, hemoglobin, and water can also influence light absorption, which means that unwanted heating in normal tissues could occur.[25,26]

Magnetic nanoparticles exposed to alternating magnetic fields enable the transformation of electromagnetic energy into heat, providing a local heat source for applications such as hyperthermia cancer treatment and polymerase chain reaction

Received: June 15, 2022
Accepted: August 14, 2022
Published: August 29, 2022

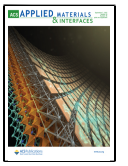

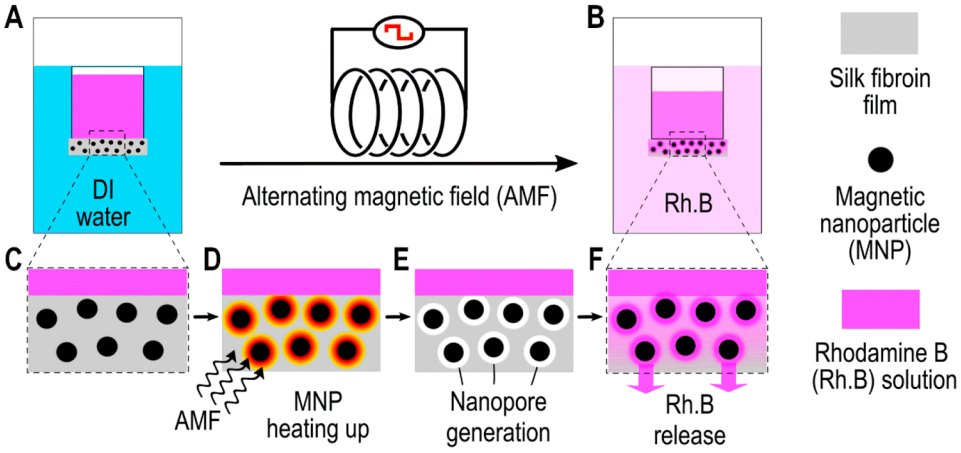

Figure 1. Silk/magnetic nanoparticles (silk/MNPs) composite membrane for controllable drug delivery with rhodamine (Rh.B) fluorescent dye as the model drug. (A) A reservoir filled with a Rh.B solution is sealed with the silk/MNP composite membrane and immersed in DI water. (B) After an alternating magnetic field (AMF) is applied, Rh.B release is triggered. (C) High-magnification image showing the cross-sectional view of the membrane composed of silk fibroin and magnetic nanoparticles. The detailed release mechanism is as follows. (D) Upon exposure to an AMF, the magnetic nanoparticles are locally heated and (E) generate nanopores in the surrounding silk fibroins, (F) which facilitate the release of the Rh.B dye solution through the composite membrane.

(PCR).[27−30] Low-frequency magnetic fields have much larger penetration depths and are capable of passing through the human body, which makes them more efficient than electromagnetic waves in the visible range as a wireless trigger for in vivo applications. Among all of the different species of magnetic nanoparticles, iron oxides are the most commonly used not only because of their ease of synthesis but also, more importantly, because of their excellent biocompatibility. It has been shown, for instance, that iron oxide nanoparticles can be metabolized by heme oxygenase-1 to form blood hemoglobin.[31]

In our previous work, a thermal and pH sensitive composite membrane composed of silk fibroin, magnetic nanoparticles, and hydrogel particles was developed for on-demand drug delivery.[32] The limited biodegradability of such a membrane due to the hydrogel particles motivates us to design a fully biodegradable membrane that can be used for in vivo applications without potential complications. Here, we report original results on silk fibroin membranes with embedded iron oxide nanoparticles as fully biodegradable material for smart drug delivery implants. The working principle is shown in Figure 1. When an external alternating magnetic field is applied, the magnetic nanoparticles inside the silk fibroin membranes are locally heated and induce thermal degradation of the surrounding silk fibroin. Consequently, nanopore structures are generated, enabling the release of a rhodamine B (Rh.B) dye solution by diffusion. The Rh.B fluorescent dye is used as a model drug[33,34] to demonstrate the capability of using the silk/magnetic nanoparticle composite membrane for drug delivery applications. The results reported in this work indicate that silk fibroin membranes with embedded iron oxide nanoparticles are suitable candidates for fully biodegradable transient drug delivery implants that can be remotely triggered by a magnetic field and used in applications such as chronic pain or tumor treatment.

EXPERIMENTAL METHODS

Characterization of Magnetic Nanoparticles. The heating properties of the magnetic nanoparticles are tested with an alternating magnetic field source (MagneTherm, nanoTherics Ltd.) equipped with an optical temperature probe. First, to determine the relationship between magnetic nanoparticle (MNP) concentrations and heating properties, the temperature of a 1 mL solution of MNPs of different concentrations (1, 5, 10, 20, 30, 40, 50, 60, and 70 g L^{-1}) is monitored over time inside an alternating magnetic field of 11 mT at 534 kHz. Second, to investigate the effect of magnetic field parameters, including magnetic field frequency and strength, on the heating capabilities of magnetic nanoparticles, the temperature of a 1 mL solution of MNPs with a fixed concentration (10, 40, and 70 g L^{-1}) is recorded over time in an alternating magnetic field with all of the available conditions (i.e., magnetic field's strength and frequency) provided by the magnetic field source. The experimental setup is shown in Figure S10.

The specific absorption rate (SAR) values normalized to the iron oxide (FeO) amount, expressed as watts per gram of FeO, are calculated according to the following equation:[35]

$$\mathrm{SAR}\left(\frac{\mathrm{W}}{\mathrm{g}}\right) = \frac{C}{m}\frac{\mathrm{d}T}{\mathrm{d}t}$$

where C is the specific heat capacity of water per unit volume (4.18 J cm^{-3} K^{-1}) and m is the concentration (grams of FeO per milliliter) of magnetic material in solution. dT/dt (kelvin per second) is the initial slope of the temperature versus time curve when the magnetic field is applied.

Preparation and Characterization of Silk/MNP Composite Membranes. The silk fibroin solution is mixed with synthesized magnetic nanoparticles. Subsequently, the silk/MNP composite membranes are prepared and characterized following the same procedure that was used for the silk fibroin membranes as described in the Supporting Information.

Effect of a Magnetic Field on the Silk/MNP Composite Membrane. To determine the influence of a magnetic field on the silk/MNP composite membrane, the EtOH annealed composite membrane is exposed to an alternating magnetic field at a fixed frequency of 111 kHz and a strength of 16 mT generated by the alternating magnetic field source for different times (2, 4, and 8 h). Then, scanning electron microscopy (SEM) is used to observe the differences in their cross-sectional microstructures.

Magnetically Triggered Controllable Rhodamine B Dye Release. To prove the potential of using the silk/MNP composite membrane for controlled, magnetically triggered drug delivery applications, the Rh.B fluorescent dye is used as a model drug to study its release behavior. A 4 mm × 4 mm × 10 mm hollow reservoir with a wall thickness of 1 mm is fabricated by a three-dimensional

https://doi.org/10.1021/acsami.2c10603
ACS Appl. Mater. Interfaces 2022, 14, 40418−40426

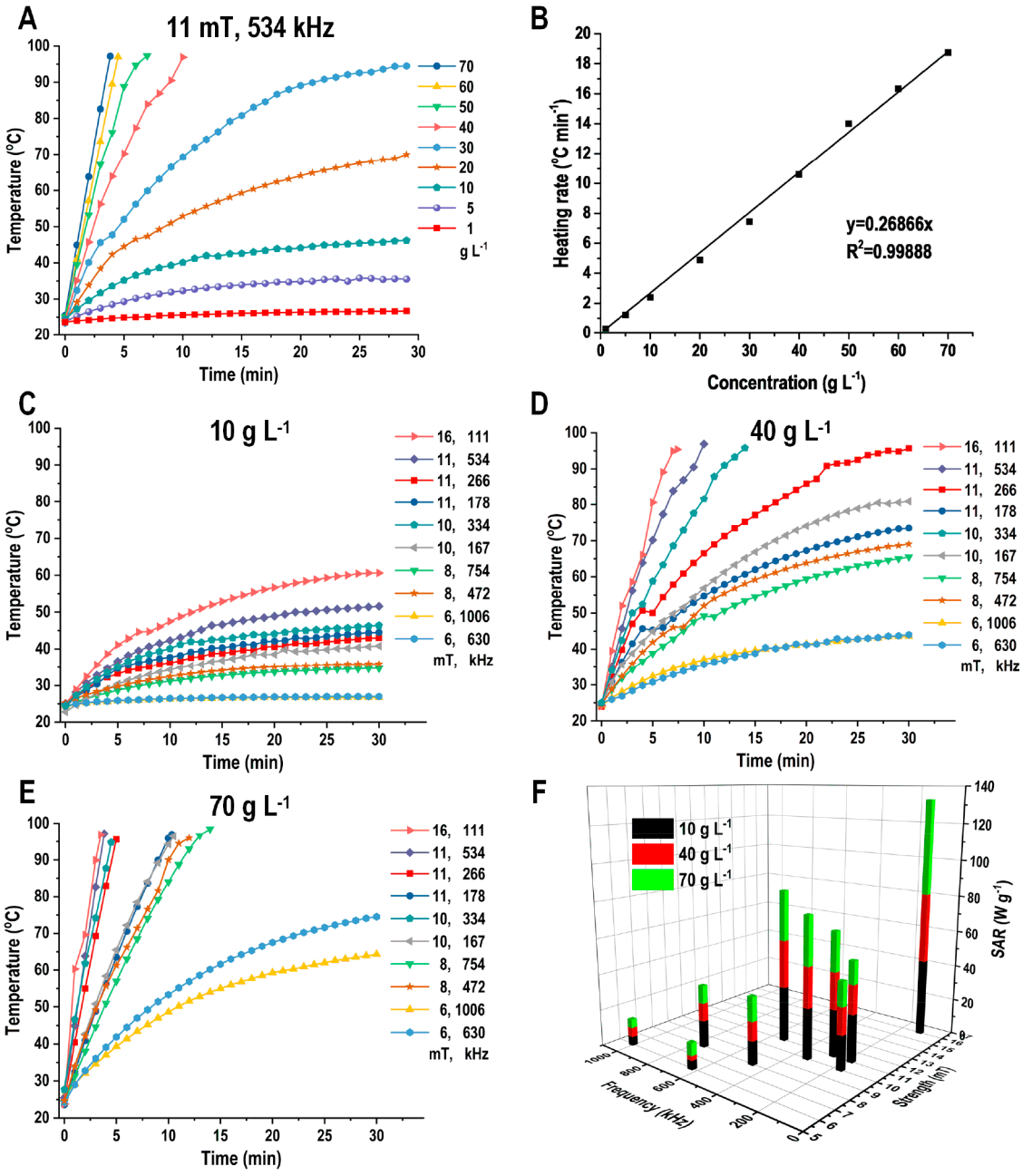

Figure 2. Analyses of the heating properties of the synthesized magnetic nanoparticles (MNPs) in water under an alternating magnetic field. (A) Time-dependent temperature profiles for MNPs solutions (1 mL) with different concentrations excited by a fixed alternating magnetic field (11 mT, 534 kHz) and (B) the corresponding relationship between the concentration of MNPs and the initial heating rate. Time-dependent temperature profiles for MNP solutions (1 mL) with concentrations of (C) 10, (D) 40, and (E) 70 g L^{-1} excited by an alternating magnetic field with different strengths and frequencies. (F) Specific absorption rate (SAR) as a function of the strength and frequency of the applied magnetic field. The results are shown in cumulative mode (e.g., the SARs for 10, 40, and 70 g L^{-1} are 43, 38, and 52 W g^{-1}, respectively, with a magnetic field of 16 mT at 111 kHz).

(3D) printer (Formlabs Clear Resin FLGPCL02). The reservoir is filled with 100 μL of a 10 g L^{-1} Rh.B solution in deionized (DI) water. A piece of silk/MNP composite membrane having a thickness of 8−10 μm and an area of ~7 mm × ~7 mm after ethanol annealing is used to seal the reservoir with glue (Scotch-Weld, 3M). The Rh.B solution-filled reservoir is placed inside a 5 mL glass vial with the composite membrane upside down to make sure that the Rh.B solution is in contact with the composite membrane. Then, 3 mL of DI water is added to ensure that the position of the composite membrane is close to the center of the solenoid coil of the alternating magnetic field source. After different periods of exposure (0, 2, 4, and 8 h) to an alternating magnetic field (16 mT, 111 kHz), the release behavior of Rh.B is monitored over time. After a certain time interval, the solution outside of the reservoir is replaced with fresh DI water (3 mL), and its absorbance at 553 nm is measured by ultraviolet−visible spectroscopy (UV−vis) (Cary 100 Bio, Varian). The calibration curve is created for the conversion of absorbance to Rh.B concentration.

RESULTS AND DISCUSSION

Thermal Heating Properties of Magnetic Nanoparticles. To investigate the heating properties of MNPs in

https://doi.org/10.1021/acsami.2c10603
ACS Appl. Mater. Interfaces 2022, 14, 40418−40426

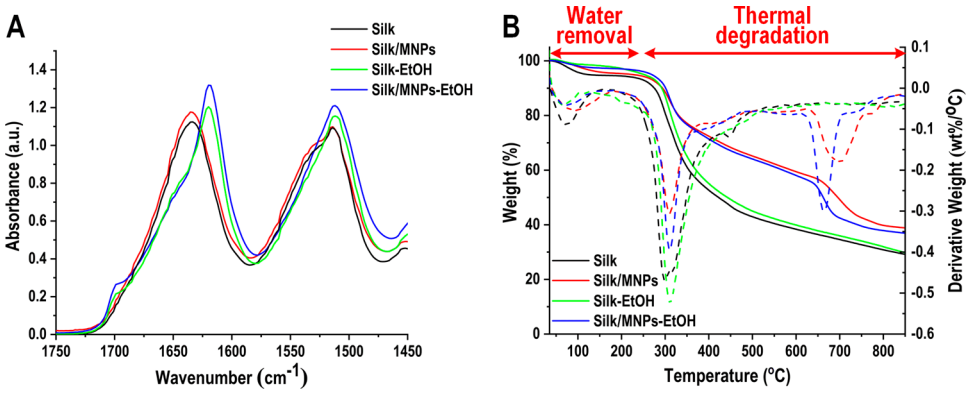

Figure 3. Study of the effects of magnetic nanoparticles on the secondary structures and thermally responsive behavior of the silk fibroin membrane. (A) Fourier-transform infrared (FTIR) spectra and (B) thermogravimetric analysis (TGA) in a N_2 atmosphere of a silk/MNP composite membrane with and without ethanol (EtOH) annealing with a bare silk fibroin membrane as a reference. The derivative thermogravimetric (DTG) curves (dashed lines) show the temperature at which water removal and degradation occur at the fastest rates.

water, magnetic heating experiments are conducted with an alternating magnetic field source (MagneTherm, nanoTherics Ltd.). In the first experiment aiming to determine the relationship between the concentration of magnetic nanoparticles and the heating efficiency, a 1 mL solution of MNPs with different concentrations is tested in an alternating magnetic field at a fixed strength (11 mT) and frequency (534 kHz). As shown in Figure 2A, for samples with lower concentrations (1−30 g L^{-1}), the temperature increases almost linearly within 3 min to 45 °C and then stabilizes gradually. For samples with higher concentrations (40−70 g L^{-1}), the temperature increases almost linearly to the water boiling temperature (i.e., 100 °C). As expected, it is found that the heating rate is higher with an increase in MNP concentration. The initial heating rates of each curve in Figure 2A are plotted against time and shown in Figure 2B. One can conclude that the heating rate increases linearly with the magnetic nanoparticle loading, whereby a maximum of 19 °C min^{-1} is measured for 70 g L^{-1} MNPs.

To further study the effect of the strength and frequency of the magnetic field on the heating rate, 1 mL solutions of MNPs with fixed concentrations of 10 g L^{-1} (Figure 2C), 40 g L^{-1} (Figure 2D), and 70 g L^{-1} (Figure 2E) are used to test the heating rate with all of the available conditions provided by the alternating magnetic field source (MagneTherm, nanoTherics Ltd.). It has been observed that the heating rate is dependent on both the magnetic field strength and the frequency (Figure 2C−E). Among all of the available conditions, the magnetic field of 16 mT at 111 kHz results in the fastest heating rate, which for MNPs with concentrations of 10, 40, and 70 g L^{-1} is 4, 15, and 37 °C min^{-1}, respectively. The heating experiments are stopped when the temperature is close to 100 °C to prevent boiling because the samples are in water. However, the temperature can actually exceed 100 °C. For example, Park et al. embedded magnetic nanoparticles in PDMS and a temperature of ∼160 °C was measured upon exposure to a magnetic field.[29]

The corresponding specific absorption rate (SAR) values as a function of the strength and frequency of the applied magnetic field for the three samples are summarized in Figure 2F. SAR provides a quantitative measure of the rate at which energy is absorbed per unit mass of the magnetic material upon exposure to a radiofrequency. The maximum SAR for MNPs obtained with a magnetic field of 16 mT at 111 kHz is 44 ± 7 W g^{-1} for MNPs with concentrations from 10 to 70 g L^{-1}. This is the condition we used for the following experiments. In magnetic hyperthermia applications, to prevent local heating in nonmagnetic tissues due to induced eddy currents, Brezovich et al. found that the product of magnetic field strength H and frequency f should be limited to $Hf < 5 \times 10^8$ A m^{-1} s^{-1}.[27] Practically, such a limit depends on the area of application in the body. Hergt et al. proposed a less rigid criterion: $Hf < 5 \times 10^9$ A m^{-1} s^{-1}.[36,37] In our case, for a magnetic field of 16 mT (i.e., 1.3×10^4 A m^{-1}) at 111 kHz, product Hf is 1.4×10^9 A m^{-1} s^{-1}, which meets the requirement for clinical applications.

Characterization of Silk/MNP Composite Membranes. Silk fibroin/magnetic nanoparticle composite membranes are prepared by the solution casting method with polyethylene Petri dishes. A polyethylene Petri dish allows an easier detachment of the membrane with respect to a standard polystyrene Petri dish. The detailed process is as follows. First, 3.5 mL of a 5 g L^{-1} MNPs solution is added dropwise to 1 mL of a 45 g L^{-1} silk fibroin solution, and the mixture is then transferred to a polyethylene Petri dish. After drying at room temperature, a silk fibroin composite membrane with 27 wt % iron oxide is obtained. The fabricated silk/MNP composite membrane is immersed in ethanol for 0.5 h and dried in the ambient atmosphere to obtain water-stable membranes.

To investigate whether the presence of magnetic nanoparticles influences the molecular structures of silk fibroin, Fourier-transform infrared (FTIR) spectroscopy is performed and the spectrum of the composite membrane is very similar to that of the pure silk fibroin membrane (Figure 3A). Before annealing, the absorbance peak is centered at ∼1635 cm^{-1}, which is the characteristic of random coil structures. After annealing, β-sheet structures form, as indicated by the absorbance peak centered at ∼1618 cm^{-1}.

Furthermore, we test the thermally responsive behavior of silk/magnetic nanoparticle (silk/MNP) composite membranes with and without EtOH annealing by thermogravimetric analysis (TGA) in a nitrogen (N_2) atmosphere. As in the case of silk without MNPs as shown in Figure 3B, there are always three stages of weight loss. The initial weight decrease is attributed to the removal of both free and bound water, which proceeds up to approximately 150 °C. The water content is ∼5 wt % for silk fibroin membranes without EtOH annealing, which is decreased to ∼2 wt % after annealing. For a silk/MNP composite membrane, there is ∼4 wt % water, which is

https://doi.org/10.1021/acsami.2c10603
ACS Appl. Mater. Interfaces 2022, 14, 40418−40426

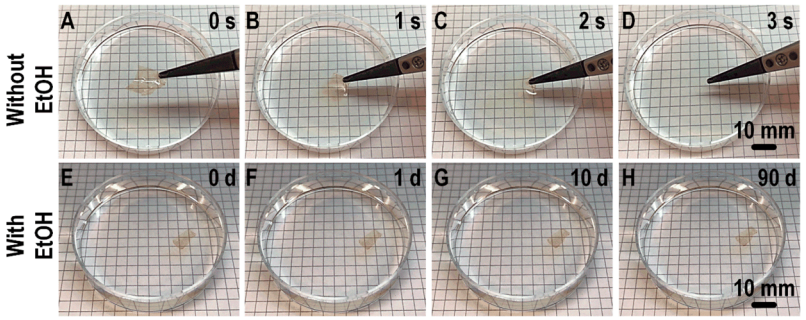

Figure 4. Stability tests of silk/MNP composite membranes in DI water (A–D) without and (E–H) with ethanol (EtOH) annealing. Without EtOH annealing, the membrane dissolves in water within 3 s. On the contrary, with EtOH treatment, the membrane is stable in water for at least 90 days.

decreased to 2 wt % after annealing. Next, the thermal degradation of silk fibroin starts with an onset temperature of ~200 °C and lasts until the end of the measurement. The strong weight loss in the temperature range of 200–550 °C is associated with the breakdown of side chain groups of silk fibroin. Without EtOH annealing, it accounts for ~54 and ~33 wt % for silk and silk/MNP composite membranes, respectively. With EtOH annealing, the losses are 55 and 36 wt % for silk and silk/MNP composite membranes, respectively. Another smaller weight loss in the range of 550–850 °C is attributed to the breakdown of main chain groups of silk fibroin. Specifically, the weight losses are ~11 and ~23 wt % for silk and silk/MNP composite membranes without EtOH annealing and 12 and 24 wt % for silk and silk/MNP composite membranes with EtOH annealing, respectively. Thus, one can conclude that the thermally responsive behavior of silk membranes is consistent, and it is affected by neither the water content and ethanol annealing nor the presence of magnetic nanoparticles.

The stability of the various silk fibroin membranes in DI water is also investigated. Without EtOH treatment, the silk/MNP composite membrane dissolves within seconds in DI water (Figure 4A–D). In contrast, for samples with EtOH treatment, they are stable in DI water for at least 1 month as shown in Figure 4E–H.

To investigate the morphologies of silk/MNP composite membranes with and without EtOH annealing, their cross-sectional surfaces are observed by SEM. For the composite membrane with EtOH annealing, a relatively flat surface with nanoparticles distributed inside it is observed (Figure 5A). A similar morphology is observed for the membrane without annealing (Figure S7A).

Effect of a Magnetic Field on the Silk/MNP Composite Membrane. To determine the influence of the magnetic field on the silk/MNP composite membrane, their morphology changes are imaged by SEM after different periods of exposure (2, 4, and 8 h) to an alternating magnetic field (16 mT, 111 kHz). As shown in Figure 5B, after exposure for 2 h, the internal structure does not show any difference compared with that of the sample not exposed to the magnetic field (Figure 5A). In particular, a similar flat surface with embedded nanoparticles is observed. In contrast, with an increase in the exposure time to 4 h, as shown in Figure 5C, nanopores are observed. After exposure to the magnetic field for 8 h, the number of nanopores created substantially increases (Figure 5D). The cross-sectional SEM images show that nanopores can be generated inside the silk/MNP composite membrane by an externally applied magnetic field. The period of exposure to the magnetic field determines reproducibly the density of the nanopores. A longer exposure time results in a larger number of nanopores. To understand more clearly the influence of the magnetic field exposure time on the silk/MNP composite membrane, a quantitative analysis of the number of nanopores is performed. In detail, the same membrane is imaged by SEM at different locations at the same magnification (the image area is 2 μm × 1.5 μm), the number of nanopores for each image is counted, and the average results are shown in Figure 5E. There is no nanopore inside the membrane after exposure for 2 h, and 17 ± 3 nanopores are observed in the membrane after exposure for 4 h, which is further increased to 65 ± 34 after exposure for 8 h. Meanwhile, due to the degradation of silk fibroin that contains carbon, nitrogen, and oxygen (Figure S4), the weight percentage of iron increases while the weight percentages of carbon, nitrogen, and oxygen decrease (Figure 5F and Figure S8).

Magnetically Triggered Release of Rhodamine B Dye. To demonstrate the potential application of using the fabricated silk/MNP composite membrane for drug delivery, a Rh.B fluorescent dye is used as a model drug. First, 3D-printed hollow reservoirs (Formlabs Clear Resin FLGPCL02) are filled with a Rh.B solution, and then ethanol-annealed silk/MNP composite membranes with 27 wt % magnetic nanoparticles are used to seal the reservoirs. Subsequently, the alternating magnetic field (16 mT, 111 kHz) is applied to trigger the heating of the magnetic nanoparticle for generating nanopores inside the composite membranes so that the Rh.B solution can diffuse across the membrane. Because, as shown by SEM (Figure 5), the number of nanopores can be controlled by adjusting the period of exposure to the magnetic field, we investigate Rh.B release behavior with membranes after exposure to the magnetic field for 0, 2, 4, and 8 h. The amount of released Rh.B is monitored by UV–vis with the calibration curve shown in Figure S6. For all four groups, the release rate of Rh.B is, as expected, very slow at the beginning, followed by an increased release rate until a plateau is reached (Figure 6). The onset of Rh.B release starts earlier for the 8 h group than for the other three groups. For the 8 h group, 1.7% Rh.B is released after 3 days, while for the other three groups, a similar released amount of Rh.B is achieved after only 7 days. More importantly, the release rate increases with the period of exposure to the magnetic field. For instance, the released amounts of Rh.B for the 0, 2, 4, and 8 h groups after 7 days are 1.8%, 1.9%, 2.4%, and 27%, respectively. After 14 days, the amounts are increased to 16%, 13%, 28%, and 74%,

https://doi.org/10.1021/acsami.2c10603
ACS Appl. Mater. Interfaces 2022, 14, 40418–40426

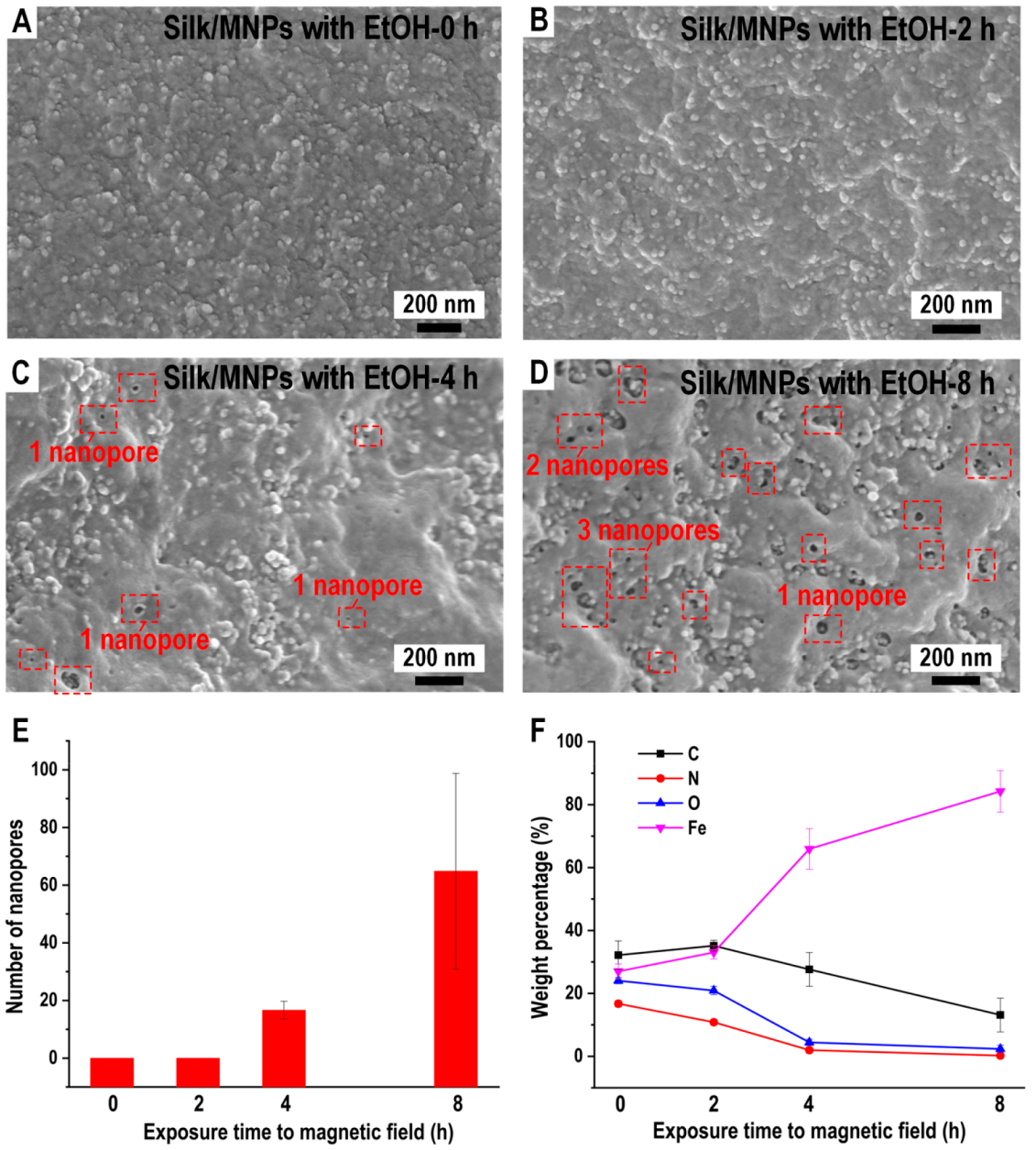

Figure 5. Investigations of the effect of an external magnetic field on the silk/MNPs composite membrane. SEM images of the cross-sectional view of EtOH-annealed silk/MNP composite membranes that have been exposed to an alternating magnetic field (16 mT, 111 kHz) for (A) 0, (B) 2, (C) 4, and (D) 8 h. (E) Number of nanopores (per an area of 2 μm × 1.5 μm) and (F) weight percentages of carbon, nitrogen, oxygen, and iron in the membranes described above as measured by energy-dispersive X-rays (EDX).

respectively, and after 21 days, the amounts are further increased to 28%, 36%, 57%, and 91%, respectively. To achieve 90% Rh.B release requires 63 days for the 0 and 2 h groups, 36 days for the 4 h group, and 20 days for the 8 h group. In conclusion, the Rh.B release rate is quite similar for the 0 and 2 h groups, which is the slowest among the tested groups, the 4 h group has a moderate release rate, and the fastest one comes from the longest exposure time (8 h group). This observation is supported by the SEM results. For membranes exposed to the magnetic field for 2 h, no nanopores could be observed, leading to Rh.B release behavior that is very close to that measured for the membrane that is not exposed to the magnetic field (0 h). For a longer exposure time, nanopores are generated, which facilitate the release of Rh.B. For the 8 h sample, many more nanopores are created and a faster release of Rh.B is achieved, which demonstrates the capability of using the fabricated silk/MNP composite membranes for magnetic field-triggered Rh.B release. More importantly, with a change in the period of exposure to the magnetic field, the release behavior can be controlled. In particular, with a longer exposure time, a faster release can be obtained.

It has been found that the morphology of a pure silk fibroin film after ethanol annealing does not change after immersion in water for 30 days as shown in Figure S3. Similarly, no change in thickness or weight has been observed for an ethanol-treated silk fibroin film in PBS after 14 days.[38] Kaplan et al. found that there was no decrease in filament diameter for *Bombyx mori* silkworm silk yarns after incubation in PBS for 12 weeks.[39] On

https://doi.org/10.1021/acsami.2c10603
ACS Appl. Mater. Interfaces 2022, 14, 40418−40426

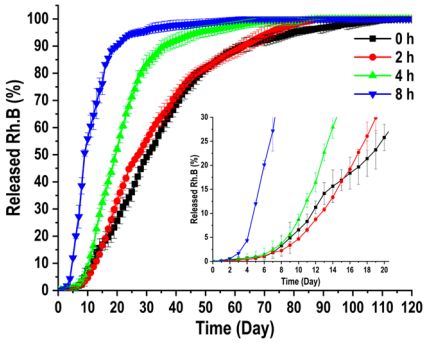

Figure 6. Controllable rhodamine B (Rh.B) release upon adjustment of the period of exposure to an alternating magnetic field. Released Rh.B through silk/MNP composite membranes vs time after different periods of exposure (0, 2, 4, and 8 h) to an alternating magnetic field (16 mT, 111 kHz). The inset shows the release profiles during the first 20 days. Data are averages ± standard deviations for three samples for each exposure time.

the basis of the findings described above, the silk fibroin film is considered to be unchanged without exposure to the magnetic field. The release of drugs embedded in a silk fibroin film is driven by diffusion through the film before the degradation starts.[40] For the model drug Rh.B encapsulated in the reservoir, it must diffuse from the inner surface of the silk fibroin film to the outer surface to be finally released into the bulk fluid. Moreover, because a silk fibroin film with magnetic nanoparticles forms a dense structure compared to the porous structure of a pure silk film, the diffusion rate is correspondingly lower and delayed. These two points lead to a delay at the initial stage of release. Once the path of diffusion is formed, the release will continue until the drug is depleted. When nanopores are generated inside the film, the diffusion path is shortened and faster release is achieved.

CONCLUSIONS

A biodegradable composite membrane composed of silk fibroin and magnetic nanoparticles has been fabricated and characterized. The realized membrane can be remotely modified by a magnetic field, allowing for controlled drug delivery applications. Ethanol annealing is used to obtain water-stable membranes by increasing the content of β-sheet structures, as confirmed by FTIR spectra. The presence of magnetic nanoparticles does not influence the secondary structures of silk fibroin. More importantly, we found by TGA that the silk/MNP composite membrane has the same thermal degradation onset temperature of ~200 °C regardless of water content, membrane thickness, annealing postprocess, and the presence of magnetic nanoparticles. We also investigated the dependence of heating rates of magnetic nanoparticles on their concentrations and the external magnetic field (strength and frequency). We observed that increasing the concentration of magnetic nanoparticles leads to a higher heating rate. The maximum heating rate achieved is 37 °C min^{-1} for 70 g L^{-1} magnetic nanoparticles upon excitation by a magnetic field of 16 mT at 111 kHz.

In particular, we demonstrate that nanopores could be generated inside the silk/MNP composite membrane after its exposure to an alternating magnetic field and that a longer exposure time results in a larger number of nanopores. With an increase in magnetic field strength, it is reasonable to expect that the period of exposure for obtaining the same amount of nanopores can be reduced. Unfortunately, the experimental setup presented here does not allow application of a magnetic field of >16 mT. An indirect proof is shown in Figure S9, in which 19 ± 9 nanopores (per an area of 2 μm × 1.5 μm) are generated after exposure to an alternating magnetic field (8 mT, 111 kHz) for 8 h. Recall that 17 ± 3 nanopores (per an area of 2 μm × 1.5 μm) are observed in the identical membrane after exposure to the magnetic field of 16 mT at 111 kHz for 4 h. With half of the magnetic field strength, we manage to obtain a similar number of nanopores by increasing the exposure time. Due to the reduced contribution of Brownian relaxation, the thermal heating efficiency of magnetic nanoparticles decreases significantly when embedded in a viscous solution,[41,42] cross-linked polymers,[43,44] and cells.[45,46] This could be one of the reasons why it needs a rather long time to generate nanopores inside the membrane, but the detailed mechanism is not yet fully understood.

The potential of applying the silk/MNP composite membrane for drug delivery is tested with Rh.B fluorescent dye as a model drug. The nanopores facilitate Rh.B passing through the membrane. With an increase in the period of exposure to the magnetic field, more nanopores are generated, and hence, a faster release of Rh.B is obtained. This indicates that the realized fully biodegradable, magnetic field responsive silk/magnetic nanoparticle composite membrane is a suitable candidate as a diffusive membrane in drug delivery implants, e.g., for chronic pain or tumor treatments.

ASSOCIATED CONTENT

Supporting Information

The Supporting Information is available free of charge at https://pubs.acs.org/doi/10.1021/acsami.2c10603.

Procedures for preparing silk fibroin membranes and silk/MNP composite membranes (Figure S1), characterizations of silk fibroin membranes by FTIR and TGA (Figure S2), stability tests of silk fibroin membranes in DI water (Figure S3), characterization of the morphology of the silk fibroin membrane by SEM (Figure S4), characterization of MNPs (Figure S5), calibration curve of a Rh.B solution (Figure S6), SEM image and EDX spectrum of the silk/MNP composite membrane without ethanol annealing (Figure S7), EDX spectra of EtOH-annealed silk/MNP composite membranes that have been exposed to an alternating magnetic field (16 mT, 111 kHz) for different times (0, 2, 4, and 8 h) (Figure S8), SEM image and EDX spectrum of EtOH-annealed silk/MNP composite membranes that have been exposed to an alternating magnetic field (8 mT, 111 kHz) for 8 h (Figure S9), and the experimental setup for magnetic heating (Figure S10) (PDF)

AUTHOR INFORMATION

Corresponding Author

Juergen Brugger − *Microsystems Laboratory, École Polytechnique Fédérale de Lausanne, 1015 Lausanne, Switzerland;* orcid.org/0000-0002-7710-5930; Email: juergen.brugger@epfl.ch

Authors

Ya Wang − *Food Science and Technology Program, Beijing Normal University-Hong Kong Baptist University United International College, 519087 Zhuhai, China; Microsystems*

https://doi.org/10.1021/acsami.2c10603
ACS Appl. Mater. Interfaces 2022, 14, 40418−40426

Laboratory, École Polytechnique Fédérale de Lausanne, 1015 Lausanne, Switzerland; orcid.org/0000-0001-5135-6339

Giovanni Boero − *Microsystems Laboratory, École Polytechnique Fédérale de Lausanne, 1015 Lausanne, Switzerland*

Xiaosheng Zhang − *School of Electronic Science and Engineering, University of Electronic Science and Technology of China, 611731 Chengdu, China*

Complete contact information is available at: https://pubs.acs.org/10.1021/acsami.2c10603

Notes

The authors declare no competing financial interest.

■ ACKNOWLEDGMENTS

This project is financially supported by the European Research Council (ERC) under the European Union's Horizon 2020 research and innovation program (Project "MEMS 4.0", ERC2016-ADG, Grant Agreement 742685), the China Scholarship Council (201306270060), the National Natural Science Foundation of China (61804023), and the Fundamental Research Funds for the Central Universities (ZYGX2019Z002).

■ REFERENCES

(1) Yi, Y.; Buttner, U.; Foulds, I. G. A Cyclically Actuated Electrolytic Drug Delivery Device. *Lab Chip* **2015**, *15* (17), 3540−3548.

(2) Caraway, D.; Walker, V.; Becker, L.; Hinnenthal, J. Successful Discontinuation of Systemic Opioids after Implantation of an Intrathecal Drug Delivery System. *Neuromodulation* **2015**, *18* (6), 508−516.

(3) Hoelzer, B. C.; Knievel, S. L.; Michiels, W. B.; McGlothlen, G. L.; Grigsby, E. J. Meningismus Associated with Malpositioned Intraspinal Catheter for Drug Delivery. *Pain Pract.* **2011**, *11* (1), 103−106.

(4) Farra, R.; Sheppard, N. F., Jr.; McCabe, L.; Neer, R. M.; Anderson, J. M.; Santini, J. T., Jr.; Cima, M. J.; Langer, R. First-in-Human Testing of a Wirelessly Controlled Drug Delivery Microchip. *Sci. Transl. Med.* **2012**, *4* (122), 122ra121.

(5) Edelhauser, H. F.; Rowe-Rendleman, C. L.; Robinson, M. R.; Dawson, D. G.; Chader, G. J.; Grossniklaus, H. E.; Rittenhouse, K. D.; Wilson, C. G.; Weber, D. A.; Kuppermann, B. D.; et al. Ophthalmic Drug Delivery Systems for the Treatment of Retinal Diseases: Basic Research to Clinical Applications. *Investig. Ophthalmol. Vis. Sci.* **2010**, *51* (11), 5403−5420.

(6) Ho, E. A.; Soo, P. L.; Allen, C.; Piquette-Miller, M. Impact of Intraperitoneal, Sustained Delivery of Paclitaxel on the Expression of P-Glycoprotein in Ovarian Tumors. *J. Controlled Release* **2007**, *117* (1), 20−27.

(7) Zachkani, P.; Jackson, J. K.; Pirmoradi, F. N.; Chiao, M. A Cylindrical Magnetically-Actuated Drug Delivery Device Proposed for Minimally Invasive Treatment of Prostate Cancer. *RSC Adv.* **2015**, *5* (119), 98087−98096.

(8) Li, Y.; Duc, H. L. H.; Tyler, B.; Williams, T.; Tupper, M.; Langer, R.; Brem, H.; Cima, M. J. In Vivo Delivery of Bcnu from a Mems Device to a Tumor Model. *J. Controlled Release* **2005**, *106* (1−2), 138−145.

(9) Lee, C. H.; Kim, H.; Harburg, D. V.; Park, G.; Ma, Y.; Pan, T.; Kim, J. S.; Lee, N. Y.; Kim, B. H.; Jang, K. I.; et al. Biological Lipid Membranes for on-Demand, Wireless Drug Delivery from Thin, Bioresorbable Electronic Implants. *NPG Asia Mater.* **2015**, *7*, No. e227.

(10) Tao, H.; Hwang, S. W.; Marelli, B.; An, B.; Moreau, J. E.; Yang, M.; Brenckle, M. A.; Kim, S.; Kaplan, D. L.; Rogers, J. A.; et al. Silk-Based Resorbable Electronic Devices for Remotely Controlled Therapy and in Vivo Infection Abatement. *Proc. Natl. Acad. Sci. U.S.A.* **2014**, *111* (49), 17385−17389.

(11) Yucel, T.; Lovett, M. L.; Kaplan, D. L. Silk-Based Biomaterials for Sustained Drug Delivery. *J. Controlled Release* **2014**, *190*, 381−397.

(12) Meinel, L.; Hofmann, S.; Karageorgiou, V.; Kirker-Head, C.; McCool, J.; Gronowicz, G.; Zichner, L.; Langer, R.; Vunjak-Novakovic, G.; Kaplan, D. L. The Inflammatory Responses to Silk Films in Vitro and in Vivo. *Biomaterials* **2005**, *26* (2), 147−155.

(13) Rockwood, D. N.; Preda, R. C.; Yucel, T.; Wang, X.; Lovett, M. L.; Kaplan, D. L. Materials Fabrication from Bombyx Mori Silk Fibroin. *Nat. Protoc.* **2011**, *6* (10), 1612−1631.

(14) Wray, L. S.; Hu, X.; Gallego, J.; Georgakoudi, I.; Omenetto, F. G.; Schmidt, D.; Kaplan, D. L. Effect of Processing on Silk-Based Biomaterials: Reproducibility and Biocompatibility. *J. Biomed. Mater. Res. B* **2011**, *99B* (1), 89−101.

(15) Gil, E. S.; Park, S. H.; Hu, X.; Cebe, P.; Kaplan, D. L. Impact of Sterilization on the Enzymatic Degradation and Mechanical Properties of Silk Biomaterials. *Macromol. Biosci.* **2014**, *14* (2), 257−269.

(16) Wenk, E.; Merkle, H. P.; Meinel, L. Silk Fibroin as a Vehicle for Drug Delivery Applications. *J. Controlled Release* **2011**, *150* (2), 128−141.

(17) Jia, L.; Ghezzi, C. E.; Kaplan, D. L. Optimization of Silk Films as Substrate for Functional Corneal Epithelium Growth. *J. Biomed. Mater. Res. B* **2016**, *104B* (2), 431−441.

(18) Lawrence, B. D.; Marchant, J. K.; Pindrus, M. A.; Omenetto, F. G.; Kaplan, D. L. Silk Film Biomaterials for Cornea Tissue Engineering. *Biomaterials* **2009**, *30* (7), 1299−1308.

(19) Kamalathevan, P.; OOi, P. S.; Loo, Y. L. Silk-Based Biomaterials in Cutaneous Wound Healing: A Systematic Review. *Advances in Skin Wound Care* **2018**, *31* (12), 565−573.

(20) Lu, Q.; Wang, X.; Hu, X.; Cebe, P.; Omenetto, F.; Kaplan, D. L. Stabilization and Release of Enzymes from Silk Films. *Macromol. Biosci.* **2010**, *10* (4), 359−368.

(21) Coburn, J. M.; Na, E.; Kaplan, D. L. Modulation of Vincristine and Doxorubicin Binding and Release from Silk Films. *J. Controlled Release* **2015**, *220*, 229−238.

(22) Kluge, J. A.; Li, A. B.; Kahn, B. T.; Michaud, D. S.; Omenetto, F. G.; Kaplan, D. L. Silk-Based Blood Stabilization for Diagnostics. *Proc. Natl. Acad. Sci. U. S. A.* **2016**, *113* (21), 5892−5897.

(23) Luo, T.; Yang, L.; Wu, J.; Zheng, Z.; Li, G.; Wang, X.; Kaplan, D. L. Stabilization of Natural Antioxidants by Silk Biomaterials. *ACS Appl. Mater. Interfaces* **2016**, *8* (21), 13573−13582.

(24) Tao, H.; Siebert, S. M.; Brenckle, M. A.; Averitt, R. D.; Cronin-Golomb, M.; Kaplan, D. L.; Omenetto, F. G. Gold Nanoparticle-Doped Biocompatible Silk Films as a Path to Implantable Thermoelectrically Wireless Powering Devices. *Appl. Phys. Lett.* **2010**, *97* (12), 123702.

(25) Ash, C.; Dubec, M.; Donne, K.; Bashford, T. Effect of Wavelength and Beam Width on Penetration in Light-Tissue Interaction Using Computational Methods. *Lasers Med. Sci.* **2017**, *32* (8), 1909−1918.

(26) Tomatsu, I.; Peng, K.; Kros, A. Photoresponsive Hydrogels for Biomedical Applications. *Adv. Drug Delivery Rev.* **2011**, *63* (14−15), 1257−1266.

(27) Deatsch, A. E.; Evans, B. A. Heating Efficiency in Magnetic Nanoparticle Hyperthermia. *J. Magn. Magn. Mater.* **2014**, *354*, 163−172.

(28) Banobre-Lopez, M.; Teijeiro, A.; Rivas, J. Magnetic Nanoparticle-Based Hyperthermia for Cancer Treatment. *Rep. Pract. Oncol. Radiother.* **2013**, *18* (6), 397−400.

(29) Kim, J. A.; Lee, S. H.; Park, H.; Kim, J. H.; Park, T. H. Microheater Based on Magnetic Nanoparticle Embedded Pdms. *Nanotechnology* **2010**, *21* (16), 165102.

(30) Zhang, H.; Huang, H.; He, S.; Zeng, H.; Pralle, A. Monodisperse Magnetofluorescent Nanoplatforms for Local Heating and Temperature Sensing. *Nanoscale* **2014**, *6* (22), 13463−13469.

(31) Corchero, J. L.; Villaverde, A. Biomedical Applications of Distally Controlled Magnetic Nanoparticles. *Trends Biotechnol.* **2009**, *27* (8), 468−476.
(32) Wang, Y.; Boero, G.; Zhang, X.; Brugger, J. Thermal and Ph Sensitive Composite Membrane for on-Demand Drug Delivery by Applying an Alternating Magnetic Field. *Adv. Mater. Interfaces* **2020**, *7* (17), 2000733.
(33) Wang, X.; Yucel, T.; Lu, Q.; Hu, X.; Kaplan, D. L. Silk Nanospheres and Microspheres from Silk/Pva Blend Films for Drug Delivery. *Biomaterials* **2010**, *31* (6), 1025−1035.
(34) Lammel, A. S.; Hu, X.; Park, S. H.; Kaplan, D. L.; Scheibel, T. R. Controlling Silk Fibroin Particle Features for Drug Delivery. *Biomaterials* **2010**, *31* (16), 4583−4591.
(35) Guardia, P.; Di Corato, R.; Lartigue, L.; Wilhelm, C.; Espinosa, A.; Garcia-Hernandez, M.; Gazeau, F.; Manna, L.; Pellegrino, T. Water-Soluble Iron Oxide Nanocubes with High Values of Specific Absorption Rate for Cancer Cell Hyperthermia Treatment. *ACS Nano* **2012**, *6* (4), 3080−3091.
(36) Muela, A.; Muñoz, D.; Martín-Rodríguez, R.; Orue, I.; Garaio, E.; Abad Díaz de Cerio, A.; Alonso, J.; García, J. Á.; Fdez-Gubieda, M. L. Optimal Parameters for Hyperthermia Treatment Using Biomineralized Magnetite Nanoparticles: Theoretical and Experimental Approach. *J. Phys. Chem. C* **2016**, *120* (42), 24437−24448.
(37) Hergt, R.; Dutz, S.; Müller, R.; Zeisberger, M. Magnetic Particle Hyperthermia: Nanoparticle Magnetism and Materials Development for Cancer Therapy. *J. Phys.: Condens. Matter* **2006**, *18* (38), S2919.
(38) Jin, H. J.; Park, J.; Karageorgiou, V.; Kim, U. J.; Valluzzi, R.; Cebe, P.; Kaplan, D. L. Water-Stable Silk Films with Reduced B-Sheet Content. *Adv. Funct. Mater.* **2005**, *15* (8), 1241−1247.
(39) Horan, R. L.; Antle, K.; Collette, A. L.; Wang, Y.; Huang, J.; Moreau, J. E.; Volloch, V.; Kaplan, D. L.; Altman, G. H. In Vitro Degradation of Silk Fibroin. *Biomaterials* **2005**, *26* (17), 3385−3393.
(40) Hines, D. J.; Kaplan, D. L. Mechanisms of Controlled Release from Silk Fibroin Films. *Biomacromolecules* **2011**, *12* (3), 804−812.
(41) Shah, R. R.; Dombrowsky, A. R.; Paulson, A. L.; Johnson, M. P.; Nikles, D. E.; Brazel, C. S. Determining Iron Oxide Nanoparticle Heating Efficiency and Elucidating Local Nanoparticle Temperature for Application in Agarose Gel-Based Tumor Model. *Mater. Sci. Eng. C Mater. Biol. Appl.* **2016**, *68*, 18−29.
(42) Rosensweig, R. E. Heating Magnetic Fluid with Alternating Magnetic Field. *J. Magn. Magn. Mater.* **2002**, *252*, 370−374.
(43) Shah, R. R.; Davis, T. P.; Glover, A. L.; Nikles, D. E.; Brazel, C. S. Impact of Magnetic Field Parameters and Iron Oxide Nanoparticle Properties on Heat Generation for Use in Magnetic Hyperthermia. *J. Magn. Magn. Mater.* **2015**, *387*, 96−106.
(44) Chen, S.; Chiang, C.; Hsieh, S. Simulating Physiological Conditions to Evaluate Nanoparticles for Magnetic Fluid Hyperthermia (Mfh) Therapy Applications. *J. Magn. Magn. Mater.* **2010**, *322* (2), 247−252.
(45) Di Corato, R.; Espinosa, A.; Lartigue, L.; Tharaud, M.; Chat, S.; Pellegrino, T.; Menager, C.; Gazeau, F.; Wilhelm, C. Magnetic Hyperthermia Efficiency in the Cellular Environment for Different Nanoparticle Designs. *Biomaterials* **2014**, *35* (24), 6400−6411.
(46) Espinosa, A.; Kolosnjaj-Tabi, J.; Abou-Hassan, A.; Plan Sangnier, A.; Curcio, A.; Silva, A. K. A.; Di Corato, R.; Neveu, S.; Pellegrino, T.; Liz-Marzán, L. M.; et al. Magnetic (Hyper)Thermia or Photothermia? Progressive Comparison of Iron Oxide and Gold Nanoparticles Heating in Water, in Cells, and in Vivo. *Adv. Funct. Mater.* **2018**, *28* (37), 1803660.

https://doi.org/10.1021/acsami.2c10603
ACS Appl. Mater. Interfaces 2022, 14, 40418−40426